# TELESEISMIC BODY WAVE ANALYSIS OF THE 1988 ARMENIAN EARTHQUAKE

J. F. Pacheco[1,2], C. H. Estabrook[1,2], D. W. Simpson[2] and J. L. Nábělek[3]

*Abstract.* Long-period and broadband body waves from 14 digital seismic stations are used to investigate the rupture process of the December 7, 1988 earthquake near Spitak, Armenia, USSR. The inversion of these data gives the following centroidal source parameters: strike 299°, dip 64°, rake 151°, depth 6.3 km and seismic moment $1.5 \times 10^{19}$ Nm, indicating that on average the earthquake had a strike-slip mechanism with a substantial reverse component. The broadband waveforms, however, show significant complexity; they are best fit with a source model that includes three sub-events, very similar in size, but with distinct focal mechanisms and locations. Rupture apparently initiated as a shallow reverse fault at a point of maximum bending on a right-lateral strike-slip fault, and then extended bilaterally, first towards the southeast and then towards the west. This interpretation agrees with the aftershock distribution and fault lineations observed on LANDSAT images.

## Introduction

Focal parameters of the devastating earthquake of December 7, 1988 near Spitak, Armenia, USSR, reported by the National Earthquake Information Center (NEIC) are: $M_S$=6.8, origin time 07h 41m 24.9s, latitude 40.987° N, longitude 44.185° E, and 10 km depth. Extensive casualties and damage occurred at the town of Spitak, just south of the epicenter, and at the city of Leninakan, near the western end of the aftershock zone (Figure 1). The rupture reached the surface south of Spitak along an approximately 8-km-long, west-northwest trending fault segment (Figure 1). The displacements along the surface trace show reverse faulting steeply-dipping to the north with a large right-lateral component: the maximum measured slip was vertically 1.6 m and laterally 0.5 m [Sharp, 1989]. The aftershock epicenters [Simpson et al., 1989] appear to divide into two groups, probably delineating at least two fault segments (Figure 1): the major segment, oriented roughly east-west, extends westward from the epicenter of the mainshock; a second segment extends from the mainshock epicenter to the southeast. The hypocenters extend to a depth of 15 km only in the west, but most occur at a depth shallower than 10 km.

The earthquake occurred along the southern edge of the Lesser Caucasus. In the Lesser and Greater Caucasus, major structures trend west-northwest and fault plane solutions indicate primarily reverse faulting [Jackson and McKenzie, 1984]. However, two moderate events ($M_W$ = 5.6 and 5.8) that occurred in 1978 and 1986 within 50 km of the Armenian earthquake epicenter, show strike-slip mechanisms with P-axes oriented north-south [Dziewonski et al., 1987a, 1987b].

The regional tectonics is characterized by north-south compression as the Arabian plate indents the Eurasian plate with a convergence velocity of 30 mm/yr across northern Iran (Figure 1). This collision results in the lateral escape of the Turkish and Iranian plates and major thrust zones, along the

[1]Department of Geological Sciences of Columbia University.
[2]Lamont-Doherty Geological Observatory.
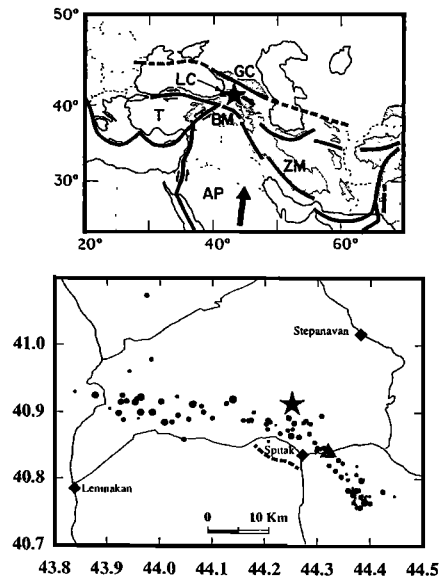[3]College of Oceanography, Oregon State University.

Fig. 1. Top figure shows NEIC location of the 1988 Armenian earthquake (star). Main plate boundaries and faults are drawn on the map as solid and dashed lines. Shaded areas are elevations higher than 2 km. Large arrow shows direction of motion of the Arabian peninsula with respect to Eurasia. LC = Lesser Caucasus, GC = Greater Caucasus, AP = Arabian plate, BM = Bitlis massif, ZM = Zagros mountains, T = Turkey. Bottom figure shows preliminary epicenters of aftershocks recorded by the U. S. Geol. Survey and Lamont-Doherty Geol. Obs. (quality a and b locations). Epicenter of main event reported by NEIC is indicated by the star, triangle shows the location from 19 local Soviet stations [Cisternas et al., 1989]. Symbol size is scaled to event magnitude, with magnitudes ranging between 1 and 4. Dashed line indicates mapped surface rupture. Thin solid lines are main roads.

Bitlis massif and Zagros mountains to the south and along the Lesser and Greater Caucasus to the north. The region between the Lesser Caucasus and the Bitlis massif is an elevated volcanic plateau with Quaternary volcanic edifices aligned in a north-south direction, suggesting an almost east-west orientation of the principal tensional axis [Kazmin et al, 1986]. The deformation here is characterized by dispersed conjugate strike-slip faults [e.g., Şengör et al., 1985].

Seismicity studies of the convergence zone [Jackson and McKenzie, 1984, 1988; Ambraseys and Adams, 1989] reveal that only a small percentage of the deformation takes place in earthquakes. Large ($M_S > 7$) historical earthquakes in the region are scarce, although an earthquake catalog compiled by Ambraseys and Adams [1989] shows several devastating earthquakes with magnitudes less than 7.

Long-period and broadband body waves recorded at 14 digital stations from the Global Digital Seismic Network (GDSN) and the Incorporated Research Institutions for Seismology (IRIS) network are used here to study the rupture process of the Armenian earthquake.

## Data and Data Analysis

The analysis of the mainshock follows procedures described by Nábělek [1984]. We use the P, SH and SV waves recorded by GDSN and IRIS stations, taking only

TABLE 1. Crustal Structure Used in Computing
Theoretical Seismograms

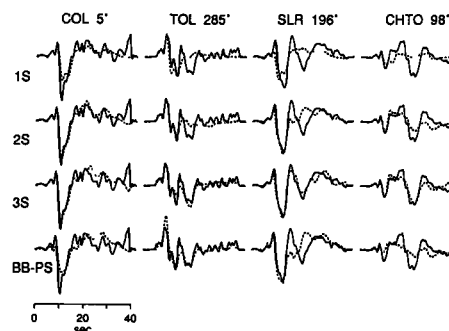|  |  | Thickness km | Vp km/s | Vs km/s | Density g/cm³ |
|---|---|---|---|---|---|
| Source |  | 1 | 4.00 | 2.14 | 2.35 |
|  |  | 5 | 5.60 | 3.23 | 2.70 |
|  |  | 30 | 6.50 | 3.75 | 2.85 |
|  |  | half-space | 8.10 | 4.68 | 3.30 |
| Receiver |  | half-space | 6.00 | 3.46 | 2.75 |



Fig. 2. Observed (solid) and theoretical (dashed) broadband seismograms for different source models from several azimuthally distributed stations. Shown are seismograms for Alaska (COL); Spain (TOL); Thailand (CHTO); and South Africa (SLR). The number next to station name is its azimuth from the source. 1S shows the effect of first subevent (see Table 2 for source parameters); 2S shows effects of subevents 1 and 2; 3S shows combined effect of 3 subevents (our final model); and BB-PS for broadband point source model.

stations in a distance range between 30° and 83° from the epicenter to avoid strong, regionally variable, upper mantle arrivals and core phases. The crustal structure (Table 1) we assumed in computing theoretical seismograms is similar to that used by Simpson et al. [1989] to locate the aftershocks. The seismograms are inverted in a least-squares sense for the source model parameters. For long-period data and intermediate magnitude earthquakes such as the Armenian earthquake, a single point source model usually provides an adequate source description. In that case, the inversion yields the average (centroidal) parameters including the fault plane solution (strike, dip, and rake of the slip direction), depth, seismic moment and time function. If required by the data, additional point sources separated in space and time can be introduced, revealing more detail about the rupture process. In this study, we started with the long-period seismograms to determine the average properties of the source, and then refined the model using the broadband records.

## Inversion Results

The results of a series of inversions we performed are summarized in Table 2. The long-period model (model LP-PS) indicates that, on average, the Armenian earthquake had a strike-slip mechanism with a large reverse-faulting component. The mean (centroid) depth is about 6 km, the seismic moment is $1.4 \times 10^{19}$ Nm, and the source duration is about 18 s. When we invert the broadband data using a single point source, we obtain essentially identical results (model BB-PS), however, the model does not provide adequate match to the data (Figure 2), indicating that the source process was more complicated. The main features of the data that the single point source model cannot adequately reproduce are the amplitudes in the early portion of the waveforms (e.g., compare BB-PS and 3S for COL in Figure 2) and the large amplitude arrival about 10 s after the first motion (e.g., SLR and CHTO). We have attempted to explain the complexity of the broadband waveforms in terms of the effects of crustal structure (Moho, low velocity layers), but such effects fail to have correct polarities, sufficient amplitudes and the required arrival times to fit the data simultaneously at all the stations. To explain these features, we were forced to subdivide the rupture into three phases. We do this by introducing three

individual point sources into our model, each having its own mechanism, time function and depth. The two point sources that describe the later part of the rupture are allowed to have arbitrary time delay and location with respect to the first. In the subsequent discussion, we will refer to the three point sources as subevents, although their contributions in most of the waveforms overlap considerably.

The parameters of the three subevents are summarized in Table 2 and the matches to the complete data set are shown in Figure 3. The initial event exhibits primarily reverse motion with a small right-lateral strike-slip component. Its mechanism is in good agreement with the mapped surface rupture. The nodal plane corresponding to the fault plane, based on field observations, strikes 299° and dips 45° northward. The mean depth of this part of the rupture is 3.1 km and the seismic moment is $5.9 \times 10^{18}$ Nm. The rupture builds up gradually and lasts for almost 9 s. The second subevent with a moment of $7.5 \times 10^{18}$ Nm locates 17 km at an azimuth of 153° relative to the first subevent (nucleation point). This subevent ruptured a nearly pure right-lateral strike-slip fault striking 309° and dipping 90°, using the aftershock distribution (Figure 1) as a guide in choosing the fault plane. The mean depth is 7.2 km and the source duration is 9 s. The third subevent has a strike-slip mechanism with a substantial reverse component and is located 38 km west of the nucleation point. The seismic moment is $5.1 \times 10^{18}$ Nm and the centroid depth is 7.3 km.

Using a moment tensor summation, the combined mechanism of the three subevents (BB-SUM, Table 2) is a pure double couple, in good agreement with that obtained by inverting the data with a single point source (BB-PS, Table

TABLE 2. Parameters of the Source Models Derived by the Inversion of Body Waves

|  | Moment 10¹⁸ Nm | Depth km | Strike deg | Dip deg | Rake deg | Duration s | Delay s | Distance km | Azimuth deg |
|---|---|---|---|---|---|---|---|---|---|
| LP-PS | 14.4 | 6.3* | 307 | 60 | 159 | 18 | - | - | - |
| BB-PS | 14.8 | 6.3 | 299 | 64 | 151 | 17 | - | - | - |
| BB-SUM | 14.1 | 6.0 | 293 | 67 | 141 | 18 | - | - | - |
| 1st subevent | 5.9 | 3.1 | 299 | 45 | 127 | 9 | - | - | - |
| 2nd subevent | 7.5 | 7.2 | 309 | 90 | 150 | 9 | 3.8 | 17 | 153 |
| 3rd subevent | 5.1 | 7.3 | 264 | 69 | 148 | 8 | 9.3 | 38 | 277 |

The formal uncertainties (2σ) are: depth 0.4 km, orientation 4°, duration 0.5 s, delay 0.5 s, distance 4 km, azimuth 5°, and moment 10%. LP-PS = Long-period point source, BB-PS = Broadband point source, BB-SUM = best double couple from sum of subevent moment tensors, "*" = depth fixed. Distance and azimuth of the centroids of the second and third subevents are measured with respect to the nucleation point (epicenter) of the first subevent.
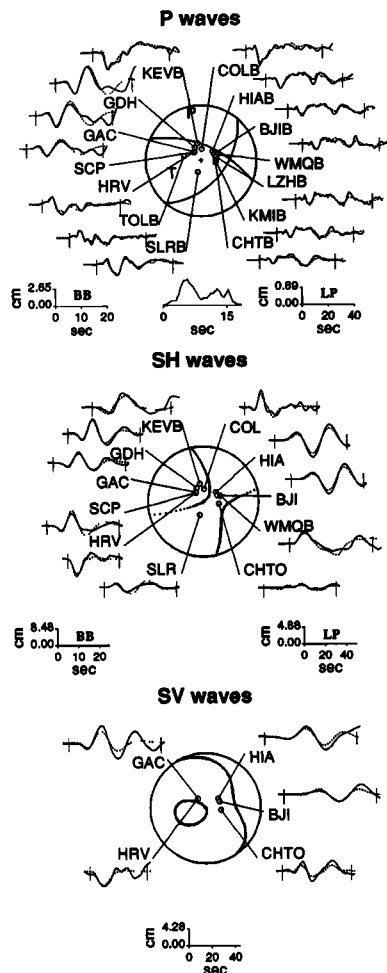
**P waves**



**SH waves**

**SV waves**

Fig. 3. Observed (solid) and theoretical (dashed) P, SH, and SV waves for best-fitting 3-subevent model (Table 2). Fault plane solution for the best double-couple of the sum of three subevents is shown at the center of the figure, and total source time function at the bottom of the P wave section. HRV and station names ending with "B" are broadband seismograms, the rest are long-period. "BB" and "LP" denote broadband and long-period scales. Seismograms are normalized to a gain of 1500 at a distance of 40°.

2). The moment released in the sequence (BB-SUM) is equivalent to an earthquake of magnitude $M_w = 6.7$.

### Discussion

The centroidal parameters of the Armenian earthquake, obtained from inversion of both the long-period and broadband data (Table 2), are well resolved and stable. On average, the earthquake had a right-lateral strike-slip mechanism with a large reverse faulting component. The orientation of the principal axes, depth of 6.0 km, and seismic moment of $1.6 \times 10^{19}$ Nm determined by the Harvard CMT method [Dziewonski et al., 1989] are very similar to those determined here. The centroid depth of the mainshock is in good agreement with average depth and extent of the aftershocks [Simpson et al., 1989]. Our centroidal results are also broadly consistent with the estimates from very-long-period (100-300 s) surface waves by Cisternas et al. [1989]. Their mechanism, however, has a somewhat steeper dipping (~70°) fault plane and the seismic moment is larger ($2 \times 10^{19}$ Nm) than ours. The higher moment estimate can probably be attributed to the difference in dip of the mechanisms and frequency of the waves. The moment release associated with

the surface rupture south of Spitak represents only about one third of the moment released during the earthquake, the rest occurred on faults at depth [see also Cisternas et al., 1989; Stein and Yeats, 1989].

The predominantly strike-slip mechanisms of the Armenian earthquake and the prior smaller earthquakes in the region indicate that the strike-slip mode of deformation in eastern Turkey and western Iran extends at least partly into the Lesser Caucasus as the material is squeezed laterally from the vise formed by the north-south collision of Arabia with Eurasia.

To explain the broadband data, we subdivided the model into three subevents corresponding to three stages of the rupture process. The mechanism of the first subevent indicates that the rupture initiated on a reverse fault. The fault strike and the sense of slip for the first subevent are consistent with the surface break mapped south of Spitak. The shallower depth of this subevent with respect to the other two, and perhaps also the difference in mechanism, may explain why only this part of the rupture reached the surface. The seismic moment estimated from the field measurements (the vertical slip of 1.6 m; lateral slip of 0.5 m; fault length of 8 km; and width of 8.8 km, based on the seismologically determined fault dip and centroid depth of 3.1 km) is $3.5 \times 10^{18}$ Nm, which is somewhat smaller than the moment we deduced for the first subevent. This indicates that the faulting corresponding to the first subevent extended beyond the surface fault break, probably westward, eventually triggering the third subevent. The duration of the first subevent is at least 9 s, considerably longer than would be needed under normal circumstances to rupture an 8 km segment.

The second stage of the rupture initiated 4 s after the earthquake origin time, before the first stage came to completion. The mechanism of the second subevent and its position to the southeast with respect to the first subevent indicate that this rupture was associated with right-lateral strike-slip faulting on a northwest-southeast striking fault, which appears to be delineated by the aftershocks and a pronounced topographic valley to the southeast of the epicenter (Figure 4). Because the first and second subevents overlap in time, the derived parameters trade-off to some extent with each other (for example, it is possible that the second subevent includes effects of some strike-slip faulting on the westward part of first event's rupture). However, the agreement of our teleseismically derived parameters with the field observations and the aftershock distribution adds confidence to our interpretation. Moreover, in spite of the differences in the faulting mechanisms, the principal compressional axes for these two subevents are oriented north-south as is generally observed for events in this area, reflecting the north-south collision of Arabia with Eurasia.

The third subevent is well separated in time from the other two and therefore its parameters are well resolved. It corresponds to strike-slip faulting at the western end of the aftershock zone. The maximum compressional axes for this mechanism, however, is rotated counter-clockwise by about 43° with respect to that of the first and second subevents, indicating that this faulting is likely to be associated with some pre-existing zone of weakness or stress redirection due to heterogeneity. Because well-located aftershocks at the western end define a clear east-west lineation following the trend of the major valley at 40.9° N, we choose the east-west striking nodal plane as corresponding to the fault plane, implying right-lateral strike-slip motion. A LANDSAT image of the region shows that, in the area where our third subevent is located, the major east-west trending valley is intersected by a second prominent valley, which may be a strike-slip fault about 25 km long with a strike of about 265° (Figure 4). The third subevent possibly occurred at the western end of the aftershock zone either on this intersecting feature or the east-west trending valley. We interpret the third subevent as faulting on a pre-existing zone of weakness, thereby explaining the difference in P axes orientation.
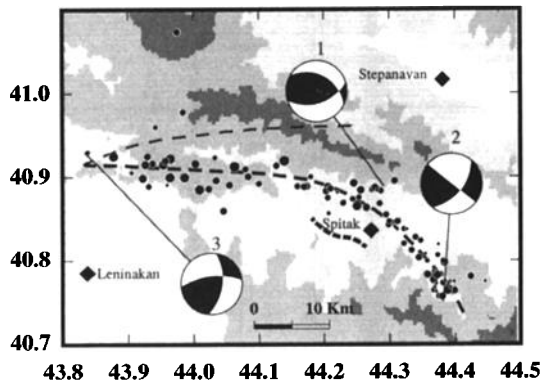
Fig. 4. Schematic showing body wave inversion results, aftershock distribution and surface rupture (small dashed line) for the Armenian earthquake. First subevent nucleated north of the town of Spitak. Centroids of the second and third subevents locate 17 km southeast and 38 km west of the first subevent, respectively. Fault plane solutions (labelled 1, 2 and 3) are those obtained in this study. Heavy dashed line drawn through the aftershocks represents the presumed fault surface at an average aftershock depth. Fault observed on LANDSAT images is shown with a thin dashed line. Shading level increases with 500 m steps in elevation.

The damage sustained at Spitak and Leninakan can be partially attributed to their proximity to the first and third subevents. Contributing factors to the destruction include the location of Spitak on the hanging wall of a shallow reverse fault and the possibility that soft sediments may have caused site amplification at Leninakan [Borcherdt et al., 1989].

Broadband seismograms have allowed us to resolve the rupture history of the Armenian earthquake with greater detail than could be done with only long-period records. The main event started at the intersection of a reverse fault with two right-lateral strike-slip faults. Four and ten seconds after nucleation, strike-slip ruptures propagated bilateraly southeast and west. This model indicates the presence of a restraining bend at the intersection of two strike-slip faults having a 45° difference in strike. The bending of the fault is also seen in the aftershock locations (Figure 1). The western end of the rupture sequence corresponds to the two valleys clearly seen in the LANDSAT image and topographic maps (Figure 4). The general scenario for the rupture process of the Armenian earthquake is in agreement with the studies by King and Nábělek [1985] and Barka and Kadinsky-Cade [1988] who showed that earthquakes often nucleate and stop near the bends and intersections of faults. The aftershock activity (Figure 4) shows concentrations at the epicenter of the mainshock and the southeastern and western ends of the fault zone, most likely indicating stress concentrations due to fault intersections.

References

Ambraseys, N. N., and R. D. Adams, Long-term seismicity of North Armenia, *EOS Transactions, A.G.U., 70*, 145-154, 1989.

Barka, A. A., and K. Kadinsky-Cade, Strike-slip fault geometry in Turkey and its influence on earthquake activity, *Tectonics, 7*, 663-684, 1988.

Borcherdt, R., G. Glassmoyer, A. Der Kiureghian and E. Cranswick, Effect of site conditions on ground motions in Leninakan, Armenia S. S. R., R. Borcherdt ed., *Results and data from seismologic and geologic studies following earthquakes of December 7, 1988, near Spitak, Armenia S. S. R. , U. S. Geological Survey Open-File Report,* 89-163A, 86-108, 1989.

Cisternas, A., et al., The Spitak (Armenia) earthquake of December 7, 1988: field observations, seismology and tectonics, *Nature, 339*, 675-679, 1989.

Dziewonski, A. M., G. Ekström, J. E. Franzen, and J. H. Woodhouse, Centroid-moment tensor solutions for April-June 1986, *Phys. Earth and Plan. Int., 45*, 229-239, 1987a.

Dziewonski, A. M., G. Ekström, J. E. Franzen, and J. H. Woodhouse, Global seismicity of 1978: centroid-moment tensor solutions for 512 earthquakes, *Phys. Earth and Plan. Int., 46*, 316-342, 1987b.

Dziewonski, A. M., G. Ekström, J. H. Woodhouse, and G. Zwart, The Armenian earthquake of 7 December 1988, *EOS Transactions, A.G.U., 70*, 394, 1989.

Jackson, J., and D. McKenzie, Active tectonics of the Alpine-Himalayan belt between western Turkey and Pakistan, *Geophys. J. R. Astr. Soc., 77*, 185-264, 1984.

Jackson, J., and D. McKenzie, The relationship between plate motions and seismic moment tensors, and the rates of active deformation in the Mediterranean and Middle East, *Geophys. J. R. Astr. Soc., 93*, 45-73, 1988.

Kazmin, V. G., I. M. Sbortshikov, L-E. Ricou, L. P. Zonenshain, J. Boulin, and A. L. Knipper, Volcanic belts as markers of the Mesozoic-Cenozoic active margin of Eurasia, *Tectonophysics, 123*, 123-152, 1986.

King, G., and J. Nábělek, Role of fault bends in the initiation and termination of earthquake rupture, *Science, 228*, 984-987, 1985.

Nábělek, J. L., Determination of earthquake source parameters from inversion of body waves, *Ph.D. Thesis*, Mass. Inst. Technol., Cambridge, Mass., pp. 361, 1984.

Sharp, R., Surface faulting investigations, R. Borcherdt ed., *Results and data from seismologic and geologic studies following earthquakes of December 7, 1988, near Spitak, Armenia S. S. R. , U. S. Geological Survey Open-File Report*, 89-163A, 21-34, 1989.

Simpson, D., C. Langer, E. Cranswick, M. Andrews, and G. Glassmoyer, Preliminary aftershock locations (December 21, 1988-January 4, 1989), R. Borcherdt ed., *Results and data from seismologic and geologic studies following earthquakes of December 7, 1988, near Spitak, Armenia S. S. R. , U. S. Geological Survey Open-File Report*, 89-163A, 75-85, 1989.

Şengör, A. M. C., N. Görür, and F. Şaroğlu, Strike-slip faulting and related basin formation in zones of tectonic escape: Turkey as a case study, K. T. Biddle and N. Christie-Blick eds., *Strike-slip deformation, basin formation, and sedimentation, Society of Economic Paleontologists and Mineralogists, special publication, 37*, 227-264, 1985.

Stein, R. S., and R. S. Yeats, Hidden earthquakes, *Sci. Am., 6*, 48, 1989.

C. H. Estabrook, J. F. Pacheco and D. W. Simpson, Lamont-Doherty Geological Observatory, Palisades, NY 10964.
J. L. Nábělek, College of Oceanography, Oregon State University, Corvallis, OR 97331.